Radiation and Environmental Biophysics

A proof of principle experiment for microbeam radiation therapy at the Munich Compact Light Source

--Manuscript Draft--

Manuscript Number:	
Full Title:	A proof of principle experiment for microbeam radiation therapy at the Munich Compact Light Source
Article Type:	Original Article
Keywords:	MRT; microbeam; compact source; tumor; X-rays; growth delay
Corresponding Author:	Thomas Ernst Schmid University Hospital rechts der Isar Muenchen, GERMANY
Corresponding Author Secondary Information:	
Corresponding Author's Institution:	University Hospital rechts der Isar
Corresponding Author's Secondary Institution:	
First Author:	Annique Cornelia Dombrowsky
First Author Secondary Information:	
Order of Authors:	Annique Cornelia Dombrowsky
	Karin Burger
	Ann-Kristin Porth
	Marlon Stein
	Martin Dierolf
	Benedikt Günther
	Klaus Achterhold
	Bernhard Gleich
	Annette Feuchtinger
	Stefan Bartzsch
	Elke Beyreuther
	Stephanie E. Combs
	Franz Pfeiffer
	Jan J. Wilkens
	Thomas E. Schmid
Order of Authors Secondary Information:	
Funding Information:	Deutsche Forschungsgemeinschaft (MAP C.3.4) — Mr Thomas E. Schmid
	Deutsche Forschungsgemeinschaft (CALA) — Mr Franz Pfeiffer
Abstract:	Microbeam radiation therapy (MRT), a preclinical form of spatially fractionated radiotherapy, uses an array of microbeams of hard synchrotron X-ray radiation. Recently, compact synchrotron X-ray sources got more attention as they provide essential prerequisites for the translation of MRT into clinics while overcoming the limited access to synchrotron facilities. At the Munich Compact Light Source (MuCLS), a beamline at one of these novel compact X-ray sources, a proof of principle

	experiment was conducted applying MRT to a xenograft tumor mouse model. First, subcutaneous tumors derived from the established squamous carcinoma cell line FaDu were irradiated at a conventional X-ray tube using broadbeam geometry to determine a suitable dose range for the tumor growth delay. For irradiations at the MuCLS, FaDu tumors were irradiated with broadbeam and microbeam irradiation at integral doses of either 3 or 5 Gy and tumor growth delay was measured. Microbeams had a width of 50 μm and a center-to-center distance of 350 μm with peak doses of either 21 or 35 Gy. A dose rate of up to 5 Gy/min was delivered to the tumor. Both doses and modalities delayed the tumor growth compared to a sham-irradiated tumor. The irradiated area and microbeam pattern were verified by staining of the DNA double-strand break marker γH2AX. This study demonstrates for the first time that microbeam radiation therapy can be successfully performed in vivo at the MuCLS.

A proof of principle experiment for microbeam radiation therapy at the Munich Compact Light Source

Annique C. Dombrowsky [1,2], Karin Burger [2,3,4], Ann-Kristin Porth [2], Marlon Stein [1,2], Martin Dierolf [3,4], Benedikt Günther [3,4], Klaus Achterhold [3,4], Bernhard Gleich [4], Annette Feuchtinger [5], Stefan Bartzsch [1,2], Elke Beyreuther [6,7], Stephanie E. Combs [1,2], Franz Pfeiffer [3,4,8], Jan J. Wilkens [2,3], Thomas E. Schmid [1,2]

thomas.schmid@helmholtz-muenchen.de
0049 89318743040

1 Institute for innovative Radiotherapy, Helmholtz Zentrum München, 85764 Neuherberg, Germany

2 Department of Radiation Oncology, Technical University of Munich, Klinikum rechts der Isar, 81675 München, Germany

3 Physics Department, Technical University of Munich, 85748 Garching, Germany

4 Munich School of BioEngineering, Technical University of Munich, 85748 Garching, Germany

5 Research Unit Analytical Pathology, Helmholtz Zentrum München, 85764 Neuherberg, Germany

6 Helmholtz-Zentrum Dresden-Rossendorf, 01328 Dresden, Germany

7 OncoRay – National Center for Radiation Research in Oncology, Faculty of Medicine and University Hospital Carl Gustav Carus, Technische Universität Dresden, Helmholtz-Zentrum Dresden-Rossendorf, 01328 Dresden, Germany

8 Institut für Diagnostische und Interventionelle Radiologie, Technical University of Munich, Klinikum rechts der Isar, 81675 München, Germany

Abstract

Microbeam radiation therapy (MRT), a preclinical form of spatially fractionated radiotherapy, uses an array of microbeams of hard synchrotron X-ray radiation. Recently, compact synchrotron X-ray sources got more attention as they provide essential prerequisites for the translation of MRT into clinics while overcoming the limited access to synchrotron facilities. At the Munich Compact Light Source (MuCLS), a beamline at one of these novel compact X-ray sources, a proof of principle experiment was conducted applying MRT to a xenograft tumor mouse model. First, subcutaneous tumors derived from the established squamous carcinoma cell line FaDu were irradiated at a conventional X-ray tube using broadbeam geometry to determine a suitable dose range for the tumor growth delay. For irradiations at the MuCLS, FaDu tumors were irradiated with broadbeam and microbeam irradiation at integral doses of either 3 or 5 Gy and tumor growth delay was measured. Microbeams had a width of 50 µm and a center-to-center distance of 350 µm with peak doses of either 21 or 35 Gy. A dose rate of up to 5 Gy/min was delivered to the tumor. Both doses and modalities delayed the tumor growth compared to a sham-irradiated tumor. The irradiated area and microbeam pattern were verified by staining of the DNA double-strand break marker γH2AX. This study demonstrates for the first time that microbeam radiation therapy can be successfully performed in vivo at the MuCLS.

Keywords MRT, microbeam, compact source, tumor, X-rays, growth delay

Acknowledgements This work has been supported by the Deutsche Forschungsgemeinschaft Cluster of Excellence: Munich-Centre for Advanced Photonics as well as the Munich School of BioEngineering of the Technical University of Munich. This work was also supported by the Centre of Advanced Laser Applications with respect to resources necessary for and at the Compact Light Source.

Conflict of interest: The authors declare they have no actual or potential competing financial interests.

Introduction

Microbeam radiation therapy (MRT) is a preclinical, spatially fractionated form of radiation therapy. MRT deposits very high doses, also referred to as peak dose, in parallel and planar beams with a width of 25 to 75 µm and a spacing of 100 to 400 µm. The deposited dose between two microbeams is lower than the tolerance dose of the normal tissue. This so-called valley dose is influenced by scattering of secondary electrons and photons from adjacent peaks (Sabatasso et al. 2011).

First in vitro and in vivo experiments focusing on tumoricidal effects of spatially fractionated irradiations were performed at large synchrotron radiation facilities such as the European Synchrotron Radiation Facility in France (Bouchet et al. 2010; Gil et al. 2011; Regnard et al. 2008). Owing to their ultra-high dose rates of hundreds of Gray per second and a small beam divergence, synchrotrons are particularly suited to maintain the microbeam pattern within the tissue without blurring (Bartzsch and Oelfke 2017). Synchrotron-generated X-ray MRT induces a differential radiobiological response in tumor and normal tissues. While the normal tissue is exceptionally tolerant to the high doses in peak regions, the tumor growth is delayed and even sometimes controlled after MRT (Bouchet et al. 2010; Crosbie et al. 2010; Laissue et al. 1998; Serduc et al. 2009). The mechanisms playing a role in the differential response of tumor and normal tissue are still unknown but there is some evidence of a differential repair of the vasculature as well as bystander effects which are, at least in part, responsible for the sparing effect (Dilmanian et al. 2007).

Patients with tumors in brain or lung surrounded by radiosensitive normal tissues would especially benefit from the pronounced tissue sparing effect of MRT (Archer et al. 2017; Ibahim et al. 2014). However, the use of synchrotrons for cancer treatment with MRT in clinics is hampered by the large space requirements and their cost-intensive operation (Bartzsch and Oelfke 2017). Therefore, in recent years new compact X-ray sources were developed such as the carbon nanotube X-ray source (Hadsell et al. 2013) or the Compact Light Source (CLS) (Eggl et al. 2016). CLSs are based on the concept of inverse Compton scattering. Compton scattering is a collision between electrons and laser photons producing nearly monochromatic X-rays. The CLS, located in Garching (Germany) and manufactured by Lyncean Technologies Inc., USA, is a compact synchrotron source producing X-rays with photon energies of 15-35 keV (Burger et al. 2017; Eggl et al. 2016). The unique features of the CLS are a small circumference of the electron storage ring of 4.6 m and a short period of the laser undulator defined by the half of the laser wavelength of 0.5 µm, allowing a size of the source of about 2 x 7 m^2 (Eggl et al. 2016). Originally, the CLS was developed for pre-clinical imaging and diagnostic of pulmonary emphysema (Schleede et al. 2012b) or breast cancer (Schleede et al. 2012a) but the CLS can also be adopted for MRT due to its synchrotron-like features.

The tumoricidal effectiveness and sparing effect of MRT at compact X-ray sources seems to be comparable to previous observations made at synchrotrons. Treatment of brain tumors with MRT generated at the carbon nanotube-based X-ray source extended the lifespan of tumor-bearing animals compared to an untreated control group (Yuan et al. 2015). In contrast to MRT at synchrotrons using peak doses of more than 100 Gy (Fardone et al. 2018), even lower peak doses of 48 or 72 Gy delayed tumor growth at compact X-ray sources (Yuan et al. 2015). At the beamline of the Munich Compact Light Source (MuCLS), in vitro experiments showed an increased survival of normal tissue cells with a lower frequency of chromosomal aberrations following MRT compared to broadbeam irradiation (Burger et al. 2017).

Both compact X-ray sources (Jacquet and Suortti 2015) and synchrotrons (Prezado et al. 2009) produce X-rays with a mean energy in the keV range. Additionally, compact X-ray sources have the advantage of lower operational costs and a laboratory-sized scale. All these features render compact X-ray sources as suitable candidates for a future implementation of MRT in clinics. To embed MRT in treatment plans of cancer patients, fundamental research of biological mechanisms and dose concepts of MRT is necessary. Especially, studies using animal models at easily accessible compact sources might help to understand MRT in more detail. Here, we show the first in vivo MRT experiment at the MuCLS, a compact synchrotron X-ray source, and evaluate its tumoricidal effect in a mouse model bearing a xenograft of squamous carcinoma cells. This proof of concept study introduces a compact X-ray source at which MRT can be performed now and which can be used for MRT in vivo studies in the future.

Materials and methods

Mouse ear tumor model

All experiments were performed using female, immunocompromised, 8-10 weeks old NMRI nu/nu mice obtained from Charles River Laboratories. Mice were hosted at the experimental sites of the Klinikum rechts der Isar in Munich according to the respective institutional guidelines and the German animal welfare regulations. The animals were kept at 20-24 °C, 45-60 % relative humidity, at 12-h light-dark cycle and fed with commercial laboratory animal diet and water ad libitum. All experiments were approved by the regional animal ethics committee (project license 55.2-1-54-2531-62-2016).

Studies were carried out for the undifferentiated human head and neck cancer cell line FaDu maintained at 37 °C, 5 % CO2 in Dulbecco Modified Eagle's Medium with 1000 mg/ml glucose (Sigma-Aldrich Chemie GmbH, Munich, Germany). The media was supplemented with 10 % FBS (Roche AG, Grenzach-Wyhlen, Germany), 2 mM L-glutamine, 1 mM sodium pyruvate, 1 % Penicillin/Streptomycin (all Sigma-Aldrich Chemie GmbH, Munich, Germany) and 10 mM HEPES (Thermo Fisher Scientific, Germering, Germany).

The mouse ear tumor model was originally established by the group of Suit et al. in 1965 and recently published as suitable model for low energy irradiation by Beyreuther et al. (2017). In order to suppress the immune response, two to four days before tumor cell injection nude mice were whole-body irradiated in a specifically designed cage which allows only a two dimensional movement of the mouse. Whole-body irradiation took place with 4 Gy of 200 kVp 15 mA X-rays filtered by aluminum (Xstrahl Ltd., UK). Then, 1 µl per gram body weight of the antibiotic Convenia (Zoetis Schweiz GmbH, Zürich, Switzerland) was subcutaneously injected into the neck. For tumor cell injection, about 100,000 FaDu tumor cells were resuspended with 50 µl Matrigel (Corning, Matrigel Basement Membrane Matrix). Mice were anaesthetized intraperitoneally with a mixture of 1 mg/ml medetomidin, 5 mg/ml midazolam and 0.05 mg/ml fentanyl. About 5 µl of the ice-cooled tumor cell suspension were injected subcutaneously between the cartilage and skin at the center of the right ear. The anesthesia was antagonized by subcutaneous injection of AFN (composed of 0.5 mg/ml atipamezole, 5 mg/ml flumazenil and 3 mg/ml faloxone). Tumor growth was measured every second day using a digital caliper of 0.01 mm accuracy (DigiMax 29422, Wiha, Buchs, Switzerland). The location of the tumor at the ear allows size measurement in three dimensions. Tumor volume was determined according to the formula $V = \frac{\pi}{6} \times a \times b \times c$. The length a of the tumor was defined as the size of the tumor parallel to the main blood vessels. The width b is perpendicular to the tumor length in the plane of the mouse ear. Measuring the maximum extension out of this plane, the height c was derived. Tumors with a maximum length of 2 mm and a maximum width of 1.8 mm were included into the experiment. There were no limitations regarding tumor height. A second criterion for tumor irradiation was the color of the tumor which changed from white to red once the tumor was vascularized. Only red-colored tumors were included into the experiment.

Irradiations at a conventional X-ray tube

A pilot study was carried out to estimate X-ray doses which induce a growth delay of xenograft FaDu tumors in the ear. This study was performed at the Small Animal Radiation Research Platform (SARRP , Xstrahl Ltd., UK) using doses of 3 and 6 Gy (Oppelt et al. 2015) applying 70 kVp X-rays filtered by aluminum. Irradiation took place with a dose rate of 2.4 Gy/min. For irradiations, a round-shaped field size of 4 mm in diameter was used. The distance between target and X-ray source was 350 mm. The tumor was centered in the irradiation field and homogeneously irradiated perpendicular to the plane of the mouse ear. Dose delivery was verified using a radiochromic film (Gafchromic EBT-3, Ashland, USA). Dose values refer to mean doses over the central area of the field as measured with radiochromic film (calibrated with an ionization chamber in an open field) before the actual experiments was performed.

On day of irradiation, the tumor had to fulfill the predefined criteria for size and color. Tumor growth was determined during a follow-up period of 30 days. Volume measurements were stopped earlier if one tumor dimension reached 8 mm (abort criteria). Growth delay of irradiated tumors was compared to unirradiated control tumors. In total four FaDu tumors were irradiated, two tumors per dose respectively, and three tumors served as control.

Tumor irradiation at MuCLS and follow-up

The radiobiological effect was compared between microbeam and broadbeam irradiation by determining the radiation-induced tumor growth delay at the MuCLS situated at the Munich School of BioEngineering in Garching (Germany).

The CLS was operated with a mean energy of 25 keV X-rays having a bandwidth of 3.6 %. The distance between mouse ear and X-ray source was 4 m. The dose at the plane of the ear was calculated from the measured photon flux. For this purpose, we used an in-house built, highly transmissible intensity counter which was placed in the beam in front of the irradiation target. The intensity counter was calibrated using a photon-counting detector (Pilatus 200K, Dectris Ltd., Baden, Switzerland). The details of the technical implementation and dosimetry are reported in a separate paper (Burger et al. in preparation), basic information about the MuCLS are reported in Eggl et al. (2016).

Tumor growth delay was compared between treated animals and a sham-irradiated, control animal. On day of irradiation, the tumor had to fulfill the predefined criteria for size and color. Animals were anaesthetized as described for tumor cell injection (see section mouse ear tumor model). The ear of the anaesthetized mouse was fixed onto the mouse holder with removable tape (Fig. 1a). Additional heating to 32-33 °C allowed the maintenance of the body temperature of the anaesthetized mouse. Tumors were positioned in the middle of the irradiation field and irradiated perpendicular to the plane of the mouse ear. A positioning system allowed for accurate placement of the tumor in the X-ray beam with a circular irradiation field of 2.3 mm in diameter.

Tumor-bearing mice were randomly assigned to the following irradiation groups: sham, microbeam or broadbeam irradiation. Irradiations took place with a dose rate up to 5 Gy/min for broadbeam and 0.6 Gy/min for microbeams. Tumors were irradiated with an integral dose of either 3 or 5 Gy. These doses for broadbeam irradiations were chosen with the aim to compare the same integrated doses for broadbeam and microbeam irradiations. Therefore, tumors were irradiated with microbeams using peak doses of either 21 or 35 Gy and valley doses below 0.2 Gy, respectively. Microbeams with a width of 50 µm and a center-to-center distance of 350 µm were generated using a highly absorbing tungsten collimator with a ratio of 1/7 slit to 6/7 tungsten. The irradiation pattern and dose to each irradiated tumor was measured by a radiochromic film (Gafchromic EBT-3, Ashland) (Fig. 1b). For this, the radiochromic film was positioned behind the tumor of each mouse. Sham irradiation follows the same protocol with exception that the X-ray beam remained switched off. After irradiation the animals were retained in quarantine during the follow-up period. Tumor growth was measured as described before (see section mouse ear tumor model). Mice were euthanized as soon as the tumor length reached 8 mm (Fig. 1c).

Staining of γH2AX on histological tumor sections

To prove irradiated area and microbeam pattern additional animals were irradiated with microbeams and assigned to histological analysis. Tumor sections were stained with hematoxylin and eosin (H&E). Staining of the DNA double-strand break marker γH2AX was performed to verify irradiation side and pattern retrospectively. The treated animal was sacrificed 1 hour after microbeam irradiation when the maximum expression of γH2AX is assumed (Kinner et al. 2008). The tumor was resected and fixed in 4 % (w/v) neutrally buffered formalin, embedded in paraffin and cut into 3 µm slices for H&E staining or for immunohistochemistry. Immunohistochemical staining was performed under standardized conditions on a Discovery XT automated stainer (Ventana Medical Systems, Tucson, AZ) using rabbit anti-γH2AX (1:500, NB100384, NOVUS Biologicals, Wiesbaden, Germany) as a primary antibody and Discovery Universal (Ventana Medical Systems, Tucson, AZ) as secondary antibody. Signal detection was conducted using the Discovery® DAB Map Kit (Ventana Medical Systems, Tucson, AZ). The stained tissue sections were scanned with an AxioScan.Z1 digital slide scanner (Zeiss, Jena, Germany) equipped with a 20x magnifying objective.

Results

Pilot study for tumor growth delay after broadbeam irradiation at SARRP

Tumor cells were subcutaneously injected into the ear of NMRI nude mice. In all mice, tumors developed and grew to a size of 2 mm in diameter at which homogeneous irradiation took place. Changes in tumor volume were measured after both 3 and 6 Gy at the SARRP. Figure 2 shows the FaDu tumor growth delay over a period of

25 days. Control tumors had a volume doubling time of 2.76 ± 0.4 days. At 3 Gy tumor growth was delayed in one of two mice. Following 6 Gy broadbeam irradiation, both FaDu tumors were controlled in their growth.

From this pre-study, we concluded that, using a higher radiobiological effective X-ray radiation of 25 keV at the CLS, a dose between 3 and 5 Gy might cause a measurable tumor growth delay at the MuCLS. With the aid of the growth delay curves after broadbeam irradiation, the 15-fold of initial volume was used for calculation of the growth delay of irradiated tumors in comparison to the sham-irradiated tumor at the MuCLS.

Effect of microbeam irradiation at the MuCLS on tumor growth

For the growth delay study at the MuCLS, FaDu cells were inoculated in the mouse ears and irradiated with sham, microbeams and broadbeam using an integral dose of either 3 or 5 Gy, respectively. In 77 % of all mice, tumors became visible and grew to the particular size on day of irradiation. After irradiation, tumor growth was recorded until the tumors reached at least their 15-fold initial volume, as determined in the previous pilot study.

Figure 3 shows the tumor volume normalized to the volume at the day of irradiation over time for one mouse per treatment. The tumor growth curves were linearly interpolated. This preliminary data indicate that growth of all irradiated tumors was delayed compared to the sham-irradiated tumor. The time reaching the 15-fold initial volume increased with increasing integrated dose from 3 to 5 Gy, independently from the radiation modality. On day 21 after irradiation, the sham-irradiated tumor reached the 15-fold volume. After 3 Gy MRT and 5 Gy MRT, tumor growth was delayed and the 15-fold initial volume was reached 3.5 days and 13.5 days later, respectively, compared to the sham-irradiated tumor. For broadbeam irradiations, the 15-fold initial volume was estimated at day 30 and day 37.5 after 3 Gy and 5 Gy, respectively. This corresponds to a tumor growth delay of 9 days for 3 Gy and 16.5 days for 5 Gy. To conclude, these preliminary data show that MRT can induce a tumor growth delay and MRT studies can be performed at the MuCLS now.

γH2AX staining of a tumor after microbeam irradiation at MuCLS

Figure 4a illustrates the FaDu xenograft tumor on day of irradiation. Tumor cells were grown in nodules surrounded by matrigel, clearly separated from the surrounding tissue and above the cartilage. Figures 4b and 4c show exemplarily the microbeam pattern, observed 1 hour after microbeam irradiation of 5 Gy. The whole area of the injection side of tumor cells mixed with matrigel was irradiated with a total of eight microbeams. The lines with γH2AX stained cells clearly correlate with the used microbeam width of 50 µm. In addition, the center-to-center distance of microbeams on the immunologically stained ear sections matches with the pattern given by the tungsten collimator (beam width of 350 µm).

Discussion

This in vivo study demonstrates that microbeam irradiation can be performed at the MuCLS using a compact synchrotron X-ray source. Microbeam and broadbeam irradiations at the MuCLS were able to induce tumor growth delay using X-rays with a mean energy of 25 keV. The irradiation pattern of microbeams was confirmed by staining of γH2AX.

Our preliminary results show that the delay of tumor growth was increased after broadbeam irradiations compared to microbeam irradiations. This observation is contradicted to the well-studied advantageous effect of MRT (Dilmanian et al. 2002; Regnard et al. 2008). However, in our proof of concept study we used only one tumor-bearing mouse per treatment group which does not allow a conclusion on the tumoricidal effect of MRT. Yet, a possible explanation for the reduced inhibitory effect of microbeam irradiations on tumor growth could be the delivered peak and valley dose. At the MuCLS, FaDu tumors were irradiated with very low peak doses of either 21 or 35 Gy and a quite constant valley dose below 0.2 Gy. Most of the in vivo studies used much higher doses in the valley and peak region of around 20 Gy and several hundred Gy, respectively (Dilmanian et al. 2002; Serduc et al. 2009). Another important parameter for tumor growth inhibition is the peak-to-valley dose ratio (PVDR). The PVDR should be low in the tumor to inhibit any repair mechanisms (Prezado et al. 2009). In the MRT study of Serduc et al. (2009) PVDRs were used between 18 and 48. This is in contrast to our study applying much higher PVDRs which might contribute to a reduced tumor growth inhibition of microbeam irradiation. Another technical parameter could be the dose rate which was much lower compared to MRT studies at synchrotrons using more than 100 Gy/s (Chtcheprov et al. 2014).

However, it has been shown that high dose rates are as efficient as conventional dose rates of 0.03 Gy/s in suppression of tumor growth (Favaudon et al. 2014). Therefore, the low dose rate of 0.6 Gy/min for microbeam irradiations should not contribute to the weak tumor growth delay at the MuCLS. Nevertheless, our study showed that even with such low peak and valley doses an inhibition of tumor growth can be induced compared to the sham-irradiated tumor but in an extent which is much lower than the tumor growth inhibitory effect of broadbeam irradiations using the same integral doses. The suppression of tumor growth after microbeam irradiation with low peak doses of 48 Gy in combination with low valley doses below 5 Gy was also measured in MRT studies at a compact X-ray source. They also confirmed a decreased effect on tumor growth inhibition of microbeam irradiation compared to broadbeam irradiation (Yuan et al. 2015; Zhang et al. 2014). This less pronounced tumor growth suppression after microbeam irradiations might be attributed to bystander effects. Bystander effects are especially induced when doses below 0.5 Gy were delivered (Fernandez-Palomo et al. 2015) which was the case in regions between adjacent beams in the MuCLS study. Bystander effects are related to DNA damage (Fernandez-Palomo et al. 2015) and apoptotic cell death (Yuan et al. 2015) in the valley region. A dose below 0.2 Gy present in the valley region of irradiated tumors at the MuCLS indicates a contribution of bystander effects to the observed inhibition of tumor growth. Another finding of our study was the increased tumor growth inhibition after a high integral dose of 5 Gy compared to an integral dose of 3 Gy. It was measured for both treatment modalities. This is in line with the study of Dilmanian et al. (2002) demonstrating a higher tumor control after delivering of higher peak doses and using a constant valley dose.

In our study, tumors were irradiated with 50 µm wide microbeams which were separated by 350 µm. The paths of microbeams can be detected by staining of γH2AX which is known as DNA double-strand break marker (Fernandez-Palomo et al. 2015). The width and the spacing between two adjacent microbeams agree to the γH2AX positively stained paths on ear sections. The immunohistochemical staining of γH2AX also shows that there is no blurring of microbeams present. Blurring of microbeams, which results in broader beam widths and lower peak-to-valley dose ratios, can happen due to respiration-induced tumor motion (Chtcheprov et al. 2014). Motion effects are more likely observed when abdominal tumors (e.g. in liver or brain) are irradiated (Chtcheprov et al. 2014; Serduc et al. 2010). At synchrotrons, motion blur can be reduced due to ultra-high dose rates of more than 100 Gy/s (Chtcheprov et al. 2014). Treating different targets, motion during microbeam irradiation at low dose rates might play an important role, which has not yet been investigated.

A technical limitation of our study was the small circular irradiation field of 2.3 mm in diameter which corresponds to the maximum tumor size plus a safety margin to irradiate. This tumor size is small compared to tumor sizes which are conventionally irradiated in tumor growth delay assays in the hind limb. Subcutaneous tumors in the hind limb have typically a size of about 8 x 4 mm^2 on day of irradiation (Zlobinskaya et al. 2014). The recently developed mouse model for growth delay studies of small subcutaneous tumors is the mouse ear tumor model where tumor cells were injected subcutaneously in the ear. This mouse ear tumor model allows the irradiation of tumors with a minimum size of 2 mm (Oppelt et al. 2015). Moreover, mouse ears have the advantage of a small thickness of about 250 µm (Girst et al. 2016) which allows penetration of low energy X-rays and thus, the treatment of shallow-seated tumors. In previous studies, the mouse ear tumor model showed a stable and high tumor take rate (Beyreuther et al. 2017). A tumor take rate of around 100 % has been recorded after inoculation of FaDu cells combined with pure matrigel (Beyreuther et al. 2017). In our pilot-study, we also observed a tumor take rate of 100 %. However, it was reduced to 77 % in the growth delay study at the MuCLS. This difference could be explained by failure in handling such as a lower injected cell concentration or inadequate mixture of cell suspension before injection. A well-known drawback of the FaDu tumor mouse ear model is a high risk of secondary tumors (Beyreuther et al. 2017). In our study, secondary tumors developed at neck or base of the right ear in 20 % of all inoculated mice.

It has been shown that tumor growth can be delayed within a dose range of 3.8 to 7.9 Gy after 200 kV X-rays (Beyreuther et al. 2017). In line with these results, our study at the MuCLS demonstrates that doses of 3 and 5 Gy of broadbeam irradiations are also able to delay tumor growth at the considerably lower X-ray energy of 25 keV. The single sham-irradiated tumor at the MuCLS reached the 15-fold initial volume on day 21 after irradiation. In contrast to that, at the SARRP control tumors reached the abort criterion on day 12 for the latest. The slower tumor growth in the MuCLS study might be ascribed to a stressful handling due to transportation from the animal house to the

radiation facility and *vice versa*. Another reason for a disturbed tumor growth could be the animal housing under quarantine conditions after irradiation at the MuCLS.

The low dose rate of compact X-ray sources is often discussed as a restriction of performing MRT in mouse models (Bartzsch and Oelfke 2017; Yuan et al. 2015). The CLS can be operated with a dose rate of 0.6 Gy/min for MRT which is in a comparable range of other novel compact microbeam sources, such as the carbon nanotube-based irradiator with a dose rate of 1.2 Gy/min (Yuan et al. 2015). Due to recently installed system upgrades at the MuCLS, higher dose rates are expected for future experiments. Nevertheless, the feasible dose rates of compact X-ray sources are much lower than the ultra-high dose rates of hundreds of Gray per second typically used in MRT studies at synchrotron facilities (Fardone et al. 2018). Despite the much lower dose rate at the MuCLS, our study showed that the tumor volume growth was reduced after microbeam irradiation at both 3 and 5 Gy. It should be noted that this tumor growth inhibition is more pronounced after broadbeam irradiations at the MuCLS. For future studies, further technical improvements which are partially already implemented should achieve an increase in size of the irradiation field, higher dose rates and peak doses for comparable MRT studies at compact X-ray sources and synchrotron facilities.

In conclusion, this proof of principle experiment introduces a novel compact X-ray source for preclinical MRT studies. The tumoricidal effect of MRT, even at low peak doses, delivered by the MuCLS was clearly demonstrated but further studies are necessary. These findings deliver important insights into the necessary dose delivery of microbeam irradiations at compact microbeam sources.

Ethical approval All applicable national and institutional guidelines for the care and use of animals were followed. All procedures performed in this study involving animals were in accordance with ethical standards of the institution at which the study was conducted (project license 55.2-1-54-2531-62-2016).

References

Archer J, Li E, Petasecca M, Dipuglia A, Cameron M, Stevenson A, Hall C, Hausermann D, Rosenfeld A, Lerch M (2017) X-ray microbeam measurements with a high resolution scintillator fibre-optic dosimeter Scientific Reports 7:12450 doi:10.1038/s41598-017-12697-6

Bartzsch S, Oelfke U (2017) Line focus x-ray tubes-a new concept to produce high brilliance x-rays Physics in medicine and biology 62:8600-8615 doi:10.1088/1361-6560/aa910b and 10.1088/1361-6560/aa910b.

Beyreuther E, Bruchner K, Krause M, Schmidt M, Szabo R, Pawelke J (2017) An optimized small animal tumour model for experimentation with low energy protons PloS one 12:e0177428 doi:10.1371/journal.pone.0177428

Bouchet A, Lemasson B, Le Duc G, Maisin C, Bräuer-Krisch E, Siegbahn EA, Renaud L, Khalil E, Rémy C, Poillot C, Bravin A, Laissue JA, Barbier EL, Serduc R (2010) Preferential Effect of Synchrotron Microbeam Radiation Therapy on Intracerebral 9L Gliosarcoma Vascular Networks International Journal of Radiation Oncology*Biology*Physics 78:1503-1512 doi:10.1016/j.ijrobp.2010.06.021

Burger K, Ilicic K, Dierolf M, Gunther B, Walsh DWM, Schmid E, Eggl E, Achterhold K, Gleich B, Combs SE, Molls M, Schmid TE, Pfeiffer F, Wilkens JJ (2017) Increased cell survival and cytogenetic integrity by spatial dose redistribution at a compact synchrotron X-ray source PloS one 12:e0186005 doi:10.1371/journal.pone.0186005

Chtcheprov P, Burk L, Yuan H, Inscoe C, Ger R, Hadsell M, Lu J, Zhang L, Chang S, Zhou O (2014) Physiologically gated microbeam radiation using a field emission x-ray source array Med Phys 41:081705 doi:10.1118/1.4886015

Crosbie JC, Anderson RL, Rothkamm K, Restall CM, Cann L, Ruwanpura S, Meachem S, Yagi N, Svalbe I, Lewis RA, Williams BRG, Rogers PAW (2010) Tumor Cell Response to Synchrotron Microbeam Radiation Therapy Differs Markedly From Cells in Normal Tissues International Journal of Radiation Oncology*Biology*Physics 77:886-894 doi:10.1016/j.ijrobp.2010.01.035

Dilmanian FA, Button TM, Le Duc G, Zhong N, Pena LA, Smith JA, Martinez SR, Bacarian T, Tammam J, Ren B, Farmer PM, Kalef-Ezra J, Micca PL, Nawrocky MM, Niederer JA, Recksiek FP, Fuchs A, Rosen EM (2002) Response of rat intracranial 9L gliosarcoma to microbeam radiation therapy Neuro-oncology 4:26-38

Dilmanian FA, Qu Y, Feinendegen LE, Pena LA, Bacarian T, Henn FA, Kalef-Ezra J, Liu S, Zhong Z, McDonald JW (2007) Tissue-sparing effect of x-ray microplanar beams particularly in the CNS: is a bystander effect involved? Exp Hematol 35:69-77 doi:10.1016/j.exphem.2007.01.014

Eggl E, Dierolf M, Achterhold K, Jud C, Gunther B, Braig E, Gleich B, Pfeiffer F (2016) The Munich Compact Light Source: initial performance measures Journal of synchrotron radiation 23:1137-1142 doi:10.1107/s160057751600967x

Fardone E, Pouyatos B, Bräuer-Krisch E, Bartzsch S, Mathieu H, Requardt H, Bucci D, Barbone G, Coan P, Battaglia G, Le Duc G, Bravin A, Romanelli P (2018) Synchrotron-generated microbeams induce hippocampal transections in rats Scientific Reports 8:184 doi:10.1038/s41598-017-18000-x

Favaudon V, Caplier L, Monceau V, Pouzoulet F, Sayarath M, Fouillade C, Poupon MF, Brito I, Hupe P, Bourhis J, Hall J, Fontaine JJ, Vozenin MC (2014) Ultrahigh dose-rate FLASH irradiation increases the differential response between normal and tumor tissue in mice Science translational medicine 6:245ra293 doi:10.1126/scitranslmed.3008973

Fernandez-Palomo C, Mothersill C, Bräuer-Krisch E, Laissue J, Seymour C, Schültke E (2015) γ-H2AX as a Marker for Dose Deposition in the Brain of Wistar Rats after Synchrotron Microbeam Radiation PloS one 10:e0119924 doi:10.1371/journal.pone.0119924

Gil S, Sarun S, Biete A, Prezado Y, Sabés M (2011) Survival Analysis of F98 Glioma Rat Cells Following Minibeam or Broad-Beam Synchrotron Radiation Therapy Radiation Oncology 6:1-9 doi:10.1186/1748-717x-6-37

Girst S, Greubel C, Reindl J, Siebenwirth C, Zlobinskaya O, Walsh DW, Ilicic K, Aichler M, Walch A, Wilkens JJ, Multhoff G, Dollinger G, Schmid TE (2016) Proton Minibeam Radiation Therapy Reduces Side Effects in an In Vivo Mouse Ear Model Int J Radiat Oncol Biol Phys 95:234-241 doi:10.1016/j.ijrobp.2015.10.020

Hadsell M, Zhang J, Laganis P, Sprenger F, Shan J, Zhang L, Burk L, Yuan H, Chang S, Lu J, Zhou O (2013) A first generation compact microbeam radiation therapy system based on carbon nanotube X-ray technology Applied physics letters 103:183505 doi:10.1063/1.4826587

Ibahim MJ, Crosbie JC, Yang Y, Zaitseva M, Stevenson AW, Rogers PA, Paiva P (2014) An evaluation of dose equivalence between synchrotron microbeam radiation therapy and conventional broad beam radiation using clonogenic and cell impedance assays PloS one 9:e100547 doi:10.1371/journal.pone.0100547

Jacquet M, Suortti P (2015) Radiation therapy at compact Compton sources Phys Med 31:596-600 doi:10.1016/j.ejmp.2015.02.010

Kinner A, Wu W, Staudt C, Iliakis G (2008) Gamma-H2AX in recognition and signaling of DNA double-strand breaks in the context of chromatin Nucleic acids research 36:5678-5694 doi:10.1093/nar/gkn550

Laissue JA, Geiser G, Spanne PO, Dilmanian FA, Gebbers JO, Geiser M, Wu XY, Makar MS, Micca PL, Nawrocky MM, Joel DD, Slatkin DN (1998) Neuropathology of ablation of rat gliosarcomas and contiguous brain tissues using a microplanar beam of synchrotron-wiggler-generated X rays Int J Cancer 78:654-660 doi:10.1002/(SICI)1097-0215(19981123)78:5<654::AID-IJC21>3.0.CO;2-L

Oppelt M, Baumann M, Bergmann R, Beyreuther E, Brüchner K, Hartmann J, Karsch L, Krause M, Laschinsky L, Leßmann E, Nicolai M, Reuter M, Richter C, Sävert A, Schnell M, Schürer M, Woithe J, Kaluza M, Pawelke J (2015) Comparison study of in vivo dose response to laser-driven versus conventional electron beam Radiation and Environmental Biophysics 54:155-166 doi:10.1007/s00411-014-0582-1

Prezado Y, Fois G, Le Duc G, Bravin A (2009) Gadolinium dose enhancement studies in microbeam radiation therapy Med Phys 36:3568-3574 doi:10.1118/1.3166186

Regnard P, Le Duc G, Brauer-Krisch E, Tropres I, Siegbahn EA, Kusak A, Clair C, Bernard H, Dallery D, Laissue JA, Bravin A (2008) Irradiation of intracerebral 9L gliosarcoma by a single array of microplanar x-ray beams from a synchrotron: balance between curing and sparing Physics in medicine and biology 53:861-878 doi:10.1088/0031-9155/53/4/003

Sabatasso S, Laissue JA, Hlushchuk R, Graber W, Bravin A, Brauer-Krisch E, Corde S, Blattmann H, Gruber G, Djonov V (2011) Microbeam radiation-induced tissue damage depends on the stage of vascular maturation Int J Radiat Oncol Biol Phys 80:1522-1532 doi:10.1016/j.ijrobp.2011.03.018 and 10.1016/j.ijrobp.2011.03.018.

Schleede S, Bech M, Achterhold K, Potdevin G, Gifford M, Loewen R, Limborg C, Ruth R, Pfeiffer F (2012a) Multimodal hard X-ray imaging of a mammography phantom at a compact synchrotron light source Journal of synchrotron radiation 19:525-529 doi:10.1107/s0909049512017682

Schleede S, Meinel FG, Bech M, Herzen J, Achterhold K, Potdevin G, Malecki A, Adam-Neumair S, Thieme SF, Bamberg F, Nikolaou K, Bohla A, Yildirim AO, Loewen R, Gifford M, Ruth R, Eickelberg O, Reiser M, Pfeiffer F (2012b) Emphysema diagnosis using X-ray dark-field imaging at a laser-driven compact synchrotron light source Proc Natl Acad Sci U S A 109:17880-17885 doi:10.1073/pnas.1206684109

Serduc R, Bouchet A, Brauer-Krisch E, Laissue JA, Spiga J, Sarun S, Bravin A, Fonta C, Renaud L, Boutonnat J, Siegbahn EA, Esteve F, Le Duc G (2009) Synchrotron microbeam radiation therapy for rat brain tumor

palliation-influence of the microbeam width at constant valley dose Physics in medicine and biology 54:6711-6724 doi:10.1088/0031-9155/54/21/017

Serduc R, Brauer-Krisch E, Siegbahn EA, Bouchet A, Pouyatos B, Carron R, Pannetier N, Renaud L, Berruyer G, Nemoz C, Brochard T, Remy C, Barbier EL, Bravin A, Le Duc G, Depaulis A, Esteve F, Laissue JA (2010) High-precision radiosurgical dose delivery by interlaced microbeam arrays of high-flux low-energy synchrotron X-rays PloS one 5:e9028 doi:10.1371/journal.pone.0009028

Yuan H, Zhang L, Frank JE, Inscoe CR, Burk LM, Hadsell M, Lee YZ, Lu J, Chang S, Zhou O (2015) Treating Brain Tumor with Microbeam Radiation Generated by a Compact Carbon-Nanotube-Based Irradiator: Initial Radiation Efficacy Study Radiat Res 184:322-333 doi:10.1667/rr13919.1

Zhang L, Yuan H, Burk LM, Inscoe CR, Hadsell MJ, Chtcheprov P, Lee YZ, Lu J, Chang S, Zhou O (2014) Image-guided microbeam irradiation to brain tumour bearing mice using a carbon nanotube x-ray source array Physics in medicine and biology 59:1283-1303 doi:10.1088/0031-9155/59/5/1283

Zlobinskaya O, Siebenwirth C, Greubel C, Hable V, Hertenberger R, Humble N, Reinhardt S, Michalski D, Roper B, Multhoff G, Dollinger G, Wilkens JJ, Schmid TE (2014) The effects of ultra-high dose rate proton irradiation on growth delay in the treatment of human tumor xenografts in nude mice Radiat Res 181:177-183 doi:10.1667/rr13464.1

Fig. 1a Tumor-bearing mouse ear is fixed with tapes onto the holder. The FaDu tumor has a size of 2 mm in diameter and is red-colored on day of irradiation. **b** Radiochromic film placed behind the ear was irradiated using microbeams with an integral dose of 5 Gy. Microbeam pattern with a beam width of 50 µm and a spacing of 300 µm is visible. **c** Illustration of the tumor size at the end of the follow-up period of tumor growth delay experiment

Fig. 2 Growth delay of individual FaDu tumors without irradiation (black lines) and after broadbeam irradiation with either 3 Gy (grey lines) or 6 Gy (grey dashed lines) using 70 kVp X-rays at the SARRP

Fig. 3 Normalized tumor volumes over the follow-up period after sham irradiation (black line), microbeam irradiation (grey dashed lines) and broadbeam irradiation (grey lines) using 25 keV X-rays at the MuCLS. One mouse per treatment was monitored until the tumor reached the 15-fold initial volume

Fig. 4 Histological analysis of FaDu tumors in mouse ears after 5 Gy microbeam irradiation at the MuCLS. Ear sections were stained with (**a**) hematoxylin and eosin (10x magnification) or (**b, c**) γH2AX one hour post-irradiation. Image b has a 5x magnification. In c, the same tumor as depicted in b is shown with a higher magnification of 10x to illustrate the microbeam width of 50 µm and a separation of 300 µm. Only the part of the ear harboring the tumor is shown

Fig 1a

Click here to access/download;colour figure;Fig 1a.png

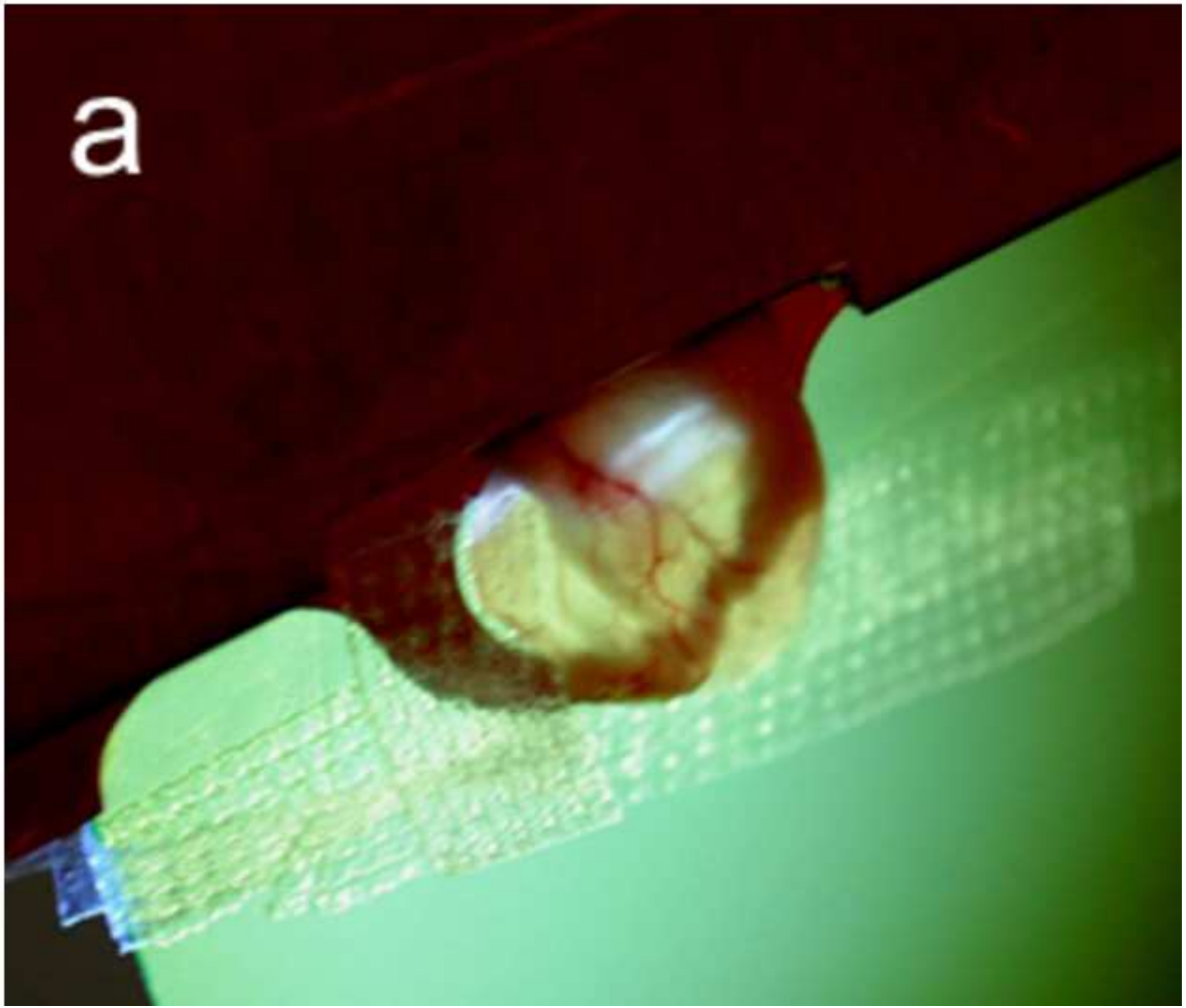

Fig 1b

Click here to access/download;colour figure;Fig 1b.png

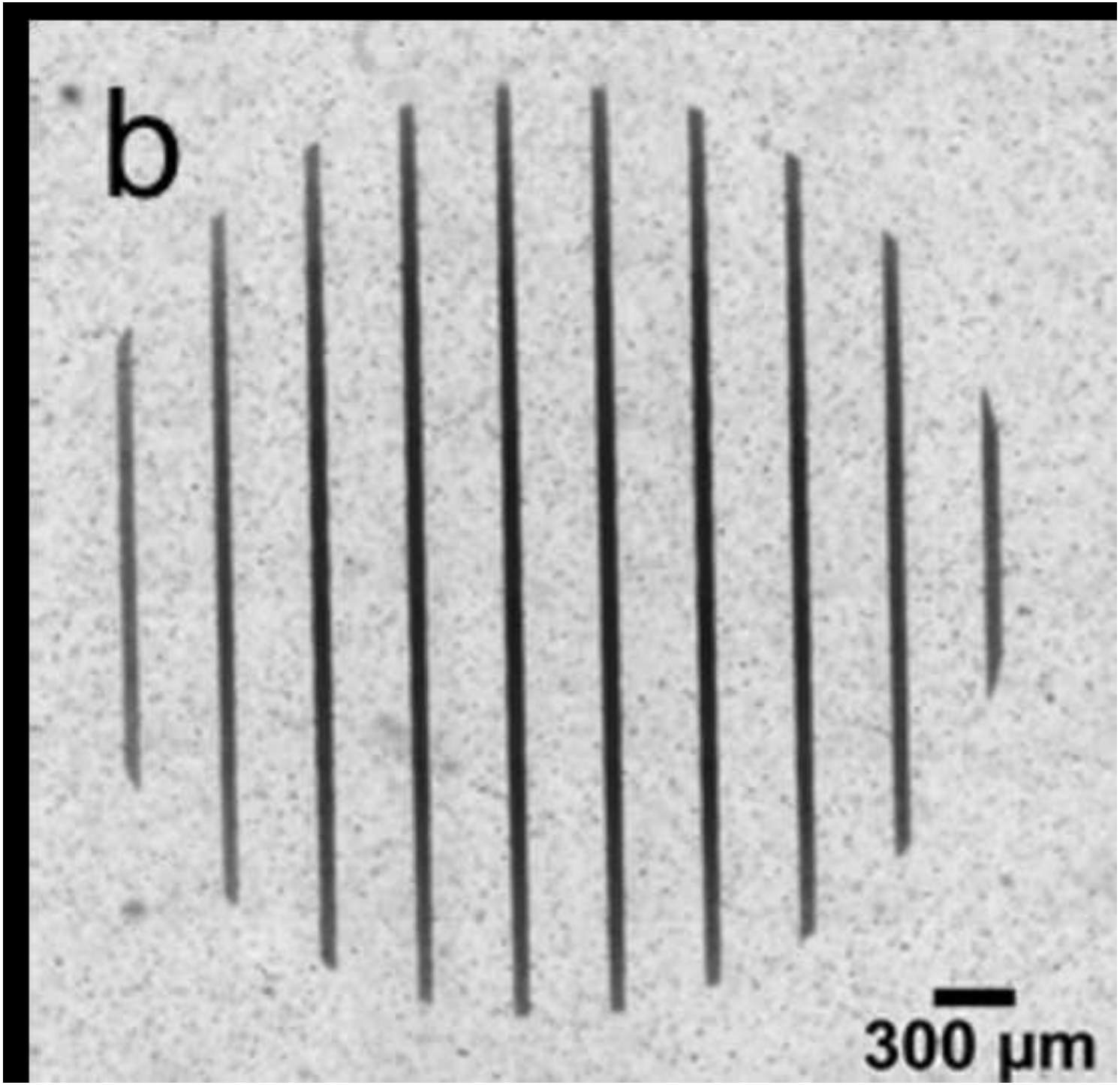

Fig 1c

Click here to access/download;colour figure;Fig 1c.png

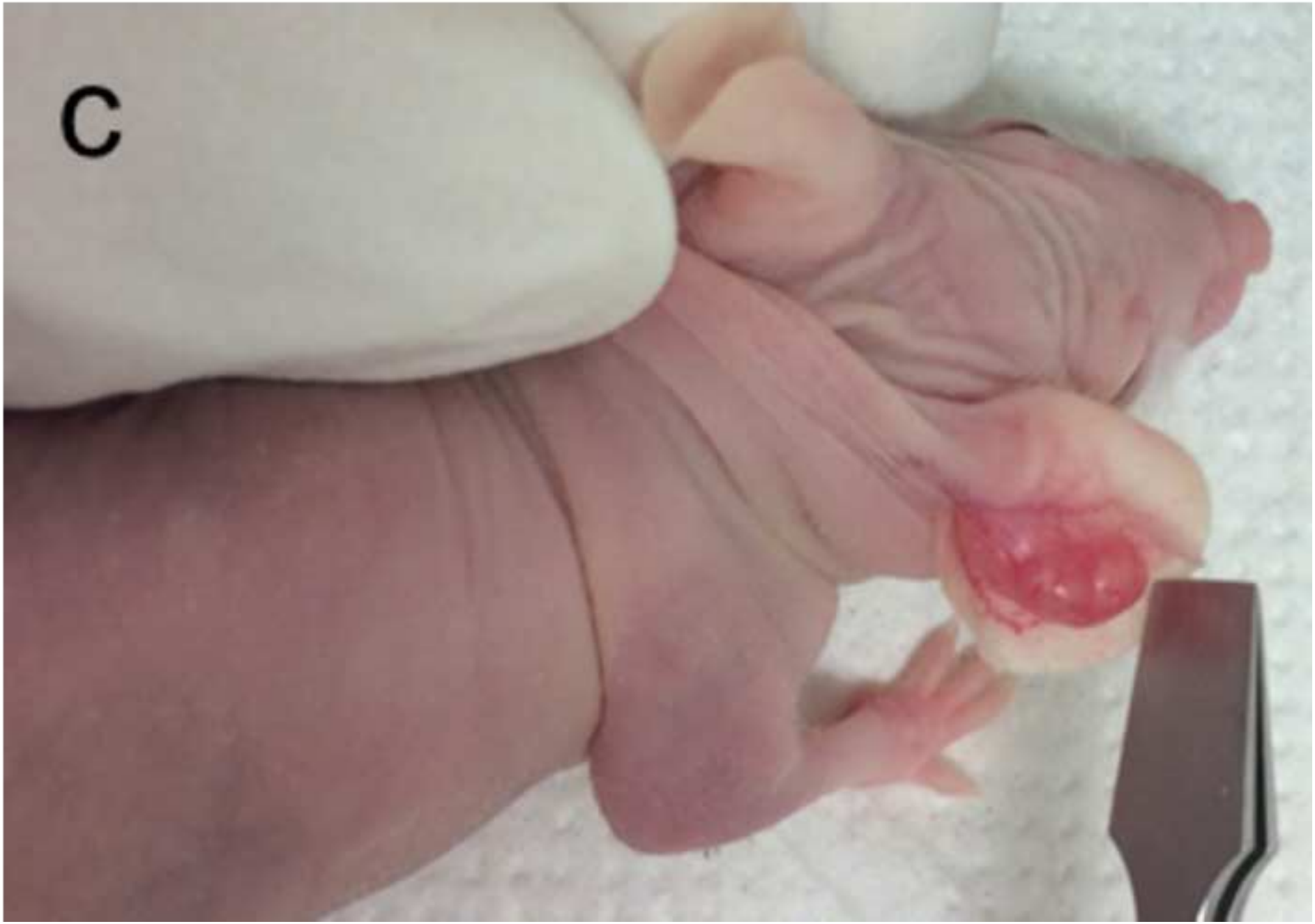

Fig 2

Click here to access/download;colour figure;Fig 2.png

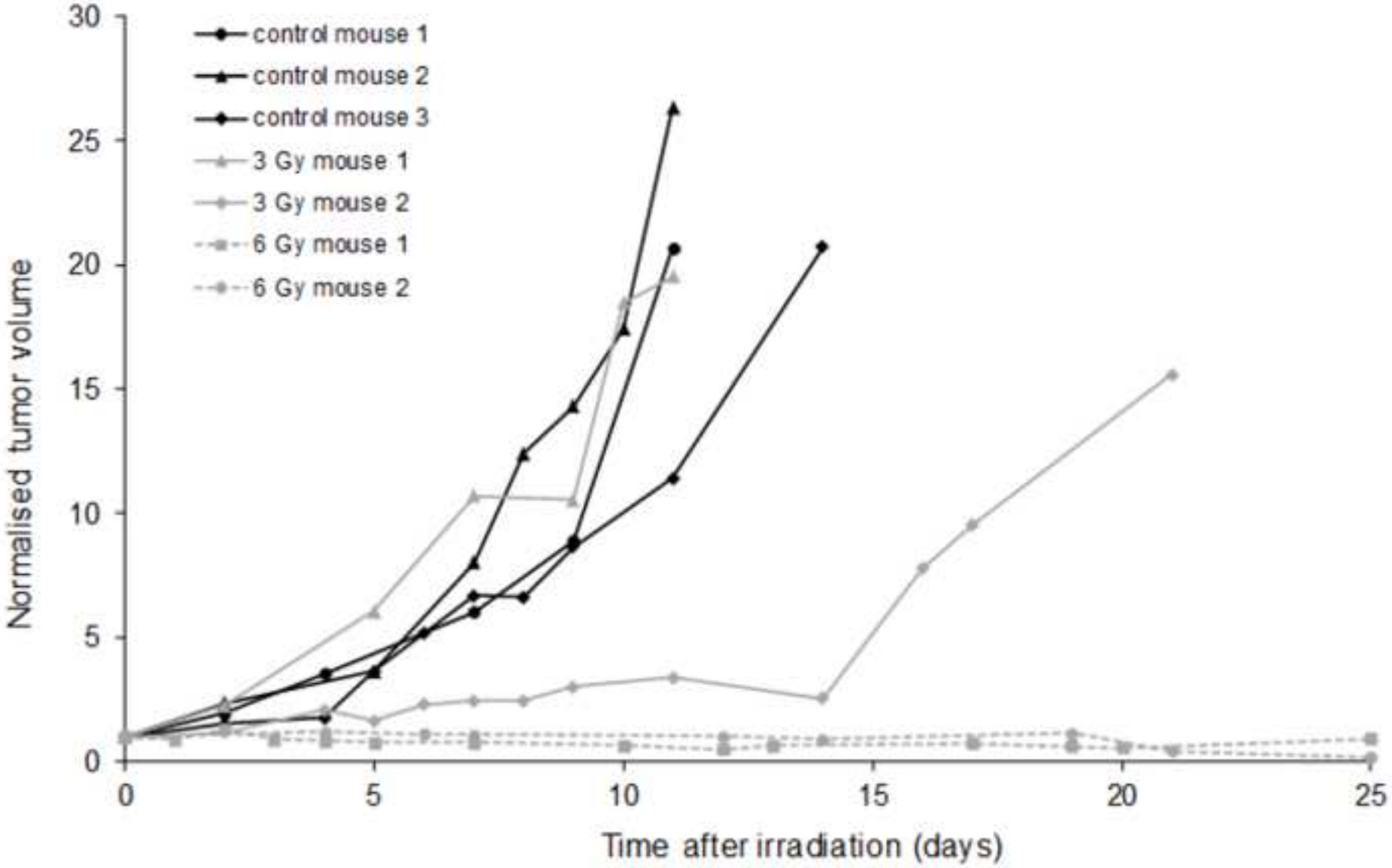

Fig 3

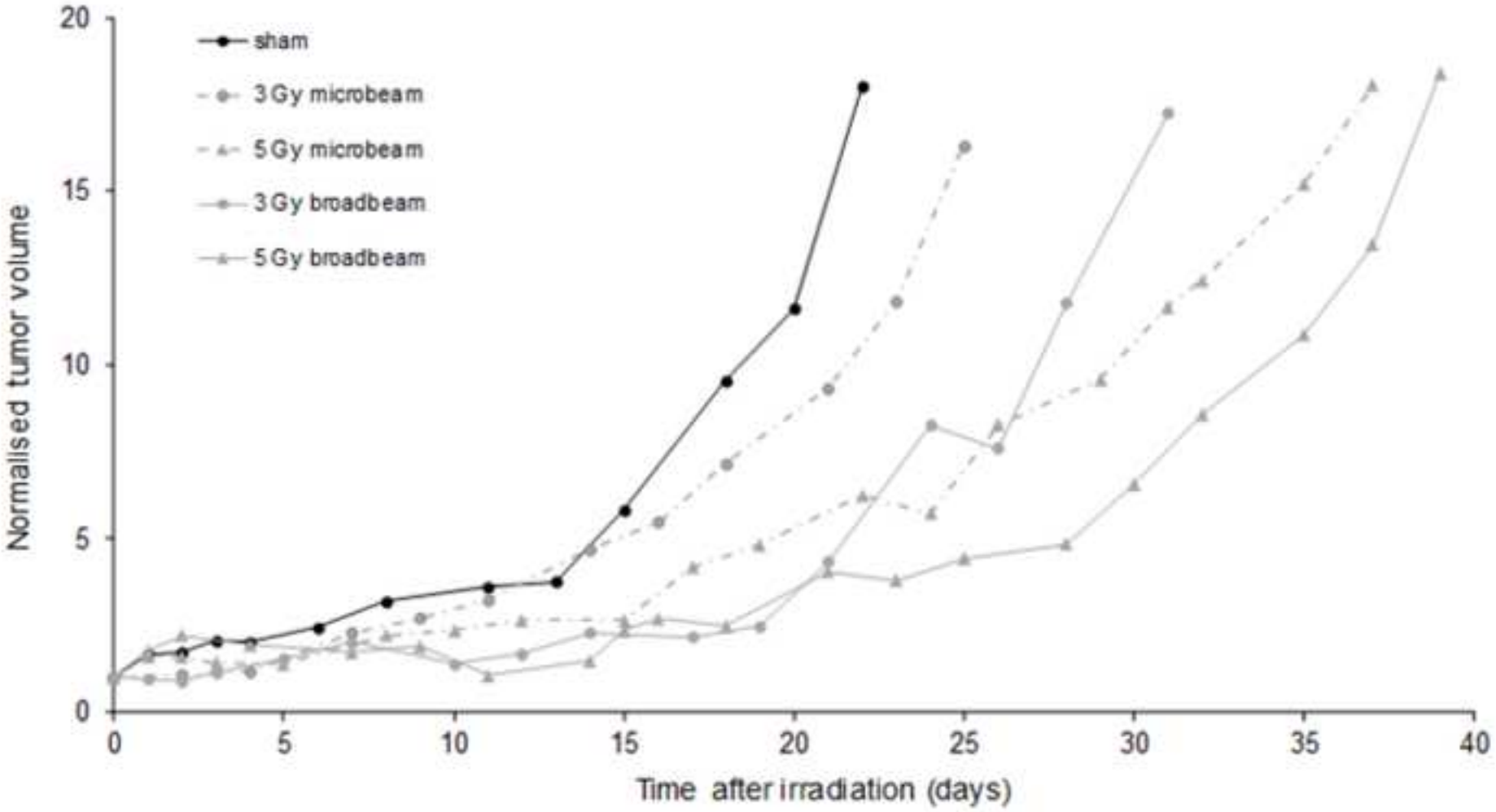

Fig 4a

Click here to access/download;colour figure;Fig 4a.jpg.png

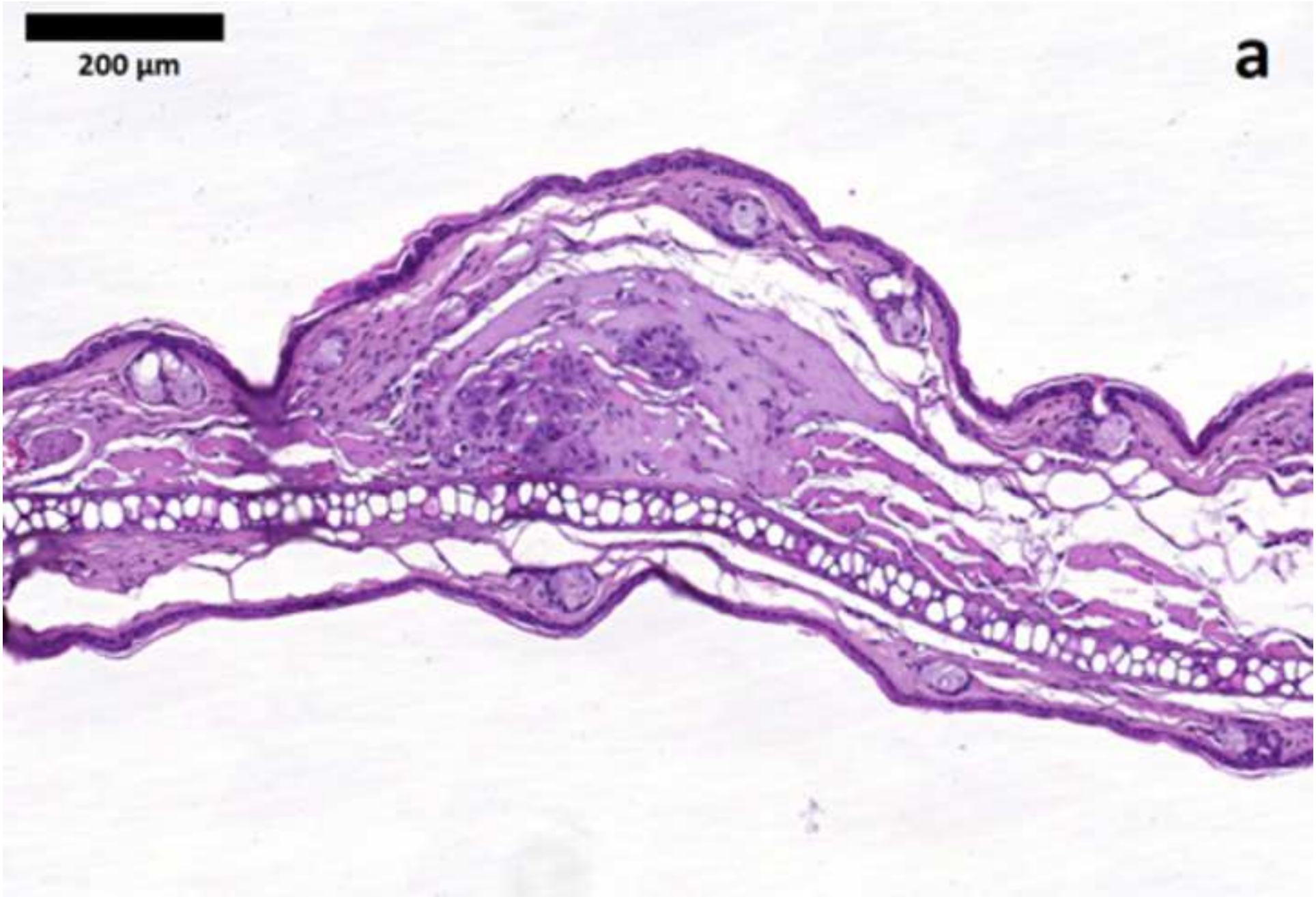

Fig 4b

Click here to access/download;colour figure;Fig 4b.jpg

Fig 4c

Click here to access/download;colour figure;Fig4c.png